Journal of the Korean Society for Nondestructive Testing
Vol. 22, No. 6 (2002. 12)

Angle Beam Ultrasonic Testing Models and Their Application to Identification and Sizing of Surface Breaking Vertical Cracks

Sung-Jin Song*,†, Hak-Joon Kim**, Hee Jun Jung* and Young H. Kim*

Abstract Identification and sizing of surface breaking vertical cracks using angle beam ultrasonic testing in practical situation quite often become very difficult tasks due to the presence of non-relevant signals caused by geometric reflectors. The present work introduces effective and systematic approaches to take care of such a difficulty by use of angle beam ultrasonic testing models that can predict the expected signals from various targets very accurately. Specifically, the model-based TIFD (Technique for Identification of Flaw signals using Deconvolution) is proposed for the identification of the crack tip signals from the non-relevant geometric reflection signals. In addition, the model-based Size-Amplitude Curve is introduced for the reliable sizing of surface breaking vertical cracks.

Keywords: ultrasonic testing, identification of flaw signals, sizing, vertical cracks, ultrasonic testing models

1. Introduction

It is widely recognized that surface breaking cracks are the most serious defects among many different kinds of flaws. Thus, they should be detected and taken care of properly for the continuing service of various parts and structures. Unfortunately, however, in many cases they grow from the inside of structures, for example, the inner surface of steel piping, where visual examination is not possible. In this situation, the angle beam ultrasonic testing (UT) is usually adopted for the detection and the further characterization of surface breaking cracks.

The characterization of a surface breaking crack by angle beam ultrasonic testing involves two steps: 1) location of the tip and the corner of the crack and 2) sizing of the crack by measuring the distance between the tip and the corner. This procedure sounds very simple and straightforward. In many practical situations, however, it is not so easy since the angle beam ultrasonic testing signals are quite often captured together with non-relevant signals caused by geometric reflectors such as corners, counter bores and weld roots. As a consequence, interpretation of the acquired signals becomes a truly difficult task so that the interpretation even by well-trained human inspectors is not reliable.

To take care of this difficulty, it is desired to have an efficient and systematic way to identifying the signals from the crack tip and the crack corner from the entire ultrasonic testing signals captured by an angle beam transducer. This paper will describe the recent progress of Sungkyunkwan University, Suwon, Korea, to address such a need.

Received September 26, 2002. * School of Mechanical Engineering, Sungkyunkwan University, Suwon, 440-746 Korea, ** Currently, Center for Nondestructive Evaluation, Iowa State University, Ames, IA 50010, USA, † Corresponding Author: sjsong@yurim.skku.ac.kr

For the reliable interpretation of angle beam ultrasonic testing, it is very beneficial to have theoretical ultrasonic testing models that can predict the UT signals from various reflectors or scatters. For this purpose, various angle beam UT models (Kim and Song, 2002; Kim et al., 2002) have been proposed by adopting the multi-Gaussian beams (Schmerr, 2000a; 2000b). These models can predict various UT signals that can be acquired from various reflectors or scatterers including the circular part of the STB A-1 block, large corners of rectangular blocks, counter bores with various sizes, vertical crack corners with various sizes, circular cracks and spherical voids. The accuracy of these models has been verified by the initial experiments.

The usage of these models is not restricted to solving the direct problem of ultrasonic testing (which is the prediction of flaw signals), but does include solving the inverse problem (which is the interpretation of flaw signals). The first application of the models to the inverse problem is related to the identification of the crack tip signal, and the second one to the sizing of vertical, surface breaking cracks.

The next section will provide brief description of the angle beam UT models developed by Sungkyunkwan University. In the following sections, the model-based identification of crack tip signals and the model-based sizing of surface breaking vertical cracks will be discussed.

2. Angle Beam Ultrasonic Testing Models

Ultrasonic testing models, which are often called as ultrasonic measurement models, are composed of four ingredients: 1) the system efficiency factor (Thompson and Gray, 1983), 2) the radiation beam field from an interrogating transducer (Song and Kim, 2000), 3) the scattering (or reflection) field from a target under consideration, and 4) the reception of scattered field by a receiving transducer. Combining of these four ingredients in a rigorous manner is very difficult. However, this difficulty can be greatly relaxed by adopting some important assumptions such as the paraxial approximation or isolated scatterer of small size.

Taking advantages of these approximations, the angle beam UT models have been developed by adopting the multi-Gaussian beams (MGBs) in the previous works (Kim and Song, 2002; Kim et al., 2002). Here, the key features of the developed models are discussed briefly to merely provide the necessary information for the present work.

2.1. Multi-Gaussian Beam Model

In the angle beam UT, ultrasonic beam propagates from a solid acrylic wedge to a solid specimen across a fluid couplant layer. Since the liquid couplant does not carry the shear waves, this propagation can be simplified to that with a fluid/solid interface, where the solid wedge is treated as a fluid medium with equivalent material properties. Then, the multi-Gaussian beam model (Schmerr, 2000a and 2000b) to calculate the transmitted beam field, $v(\omega,\mathbf{x})$, at the point x in the solid specimen (as shown in Fig. 1) can be written by Eq. (1).

$$v(\omega,\mathbf{x})=\sum_{n=1}^{N}\mathbf{d}^{\alpha}\frac{A_n}{1+\left(\frac{iB_n z_1}{z_r}\right)}T_{12}^{\alpha;p}\frac{\sqrt{\det\mathbf{G}_2^{\alpha}(0)}}{\sqrt{\det\mathbf{G}_2^{\alpha}(x_3)}}\times\exp\left(ik_2^{\alpha}x_3\right)\exp\left[\frac{ik_1\mathbf{x}^T\left[\mathbf{G}_2^{\alpha}(x_3)\right]^{-1}\mathbf{x}}{2}\right] \quad \cdots\cdots (1)$$

where ω is the circular frequency, A_n and B_n are height and width factors of individual Gaussian beams, z_1 is the distance from transducer to interface, $z_r=(1/2)k_1a^2$ is the Rayleigh distance, $T_{12}^{\alpha;p}(\alpha=P,SV)$ is the transmission coefficient, $k_1,k_2^{\alpha}(\alpha=P,SV)$ are the wave numbers in the fluid and solid, respectively. Definition of the other terms including $G_2^{\alpha}(0)$ and $G_2^{\alpha}(\chi_3)$ matrices were discussed in detail by Schmerr (2000a).

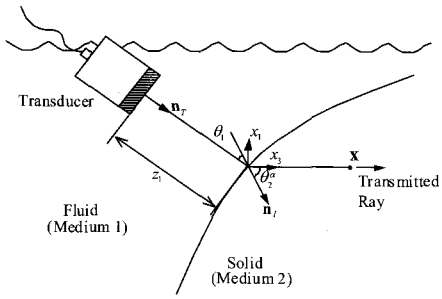

Fig. 1 Geometry of the multi-Gaussian beam model with fluid-solid interface

2.2. Reference Reflection

The reflection signal from the circular part of the STB-A1 block was chosen as a reference reflection for the estimation of the system efficiency factor, $\beta(\omega)$, of an angle beam ultrasonic testing set-up as shown in Fig. 2. Then, the reference reflection model can be written as Eq. (2).

$$V_R(\omega)=\frac{1}{S}\int_S v_R(\omega,\mathbf{x})dS \qquad \cdots\cdots (2)$$

where $V_R(\omega)$ is the received average velocity in the frequency domain, S is the transducer area, x is an arbitrary point on S, and $v_R(\omega,\mathbf{x})$ is given by Eq. (3).

$$v_R(\omega,\mathbf{x})=\sum_{n=1}^{15}\frac{A_n}{1+\left(\frac{iB_n z_1}{z_r}\right)}T_{12}^{s;p}R_{23}^{s;s}T_{21}^{p;s}\frac{\sqrt{\det\mathbf{G}_2^s(0)}}{\sqrt{\det\mathbf{G}_2^s(z_2)}}\frac{\sqrt{\det\tilde{\mathbf{G}}_3^s(0)}}{\sqrt{\det\tilde{\mathbf{G}}_3^s(z_3)}}$$
$$\times\frac{\sqrt{\det\mathbf{G}_4^s(0)}}{\sqrt{\det\mathbf{G}_4^s(z_4)}}\exp(2ik_1z_1)\exp(2ik_2^sz_2)\exp\left(\frac{ik_2^s\Phi^p(z_4)}{2}\right) \qquad \cdots\cdots (3)$$

where $T_{12}^{s;p}$ is the transmission coefficient from the wedge to the STB-A1 block, $T_{21}^{p;s}$ is the transmission coefficient from the STB-A1 block to the wedge, $R_{23}^{s;s}$ is the reflection coefficient at the circular part of STB-A1 block.

2.3. System Efficiency Factor

The system efficiency factor, $\beta(\omega)$, can be computedby use of the deconvolution of the experimental signal captured from the reference reflector (the circular part of thce STB-A1 block) by the reference reflector model (given by Eq. (2)), as given by Eq. (4)

$$\beta(\omega)=\frac{V_0(\omega)}{V_R(\omega)}W(\omega) \qquad \cdots\cdots (4)$$

where $V_0(\omega)$ is the measured voltage by the experiments, $V_R(\omega)$ is the calculated voltage by the reference model and $W(\omega)$ is the Wiener filter (Schmerr, 1998).

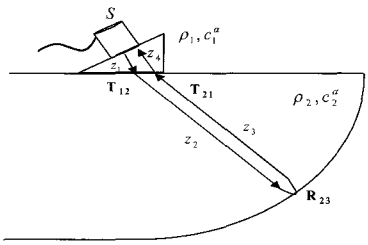

Fig. 2 Geometrical setup for the calibration of an angle beam ultrasonic transducers

2.4. Counter Bore Reflection

When the size of a counter bore is smaller than the beam width, it can be considered as a scatterer. In this case, the surface of the counter bore can be divided into small, planar elements. And, the individual responses from each element can be evaluated by use of a well-known ultrasonic measurement model, given by Eq. (5). Then, finally, the total response from the small counter bore can be obtained by summing up all the responses from individual elements.

$$V_{sb}(\omega)=\beta(\omega)\exp(2ik_1z_1)\exp(2ik_2^sz_2)$$
$$\times\left[T_{12}^{s;p}C(\omega)\right]^2A^{s;s}(\omega)\left(\frac{c_2^s}{-i\pi fa^2}\frac{\rho_2c_2^s}{\rho_1c_1}\right) \qquad \cdots\cdots (5)$$

where ρ_1,ρ_2 are density of the wedge and specimen, c_1, c_2^s are the P- and S-wave speed in the wedge and specimen, f is the frequency, a is the radius of transducer, and the far-filed scattering

amplitude, $A^{s;s}(\omega)$, from a planar crack is given by Eq. (6) based on the Kirchhoff approximation (Schmerr, 1998):

$$A^{s;s}(\omega)=\frac{-ik_2^s\left(\delta_{ln}-e_{sl}^s e_{sn}^s\right)e_{sj}^s C_{kplj} D_p^s n_k}{4\pi\rho_2\left(c_2^s\right)^2} \times \int_{S_F}\exp\left[i\left(k_2^s\mathbf{e}_i^s-k_2^s\mathbf{e}_r^s\right)\cdot\mathbf{x}_s\right]dS_F(\mathbf{x}_s) \quad \cdots\cdots (6)$$

and, the diffraction correction, $C(\omega)$, is given by Eq. (7):

$$C(\omega)=\sum_{n=1}^{15}\frac{A_n}{1+\left(\frac{iB_n z_1}{x_r}\right)}T_{12}^{s;p}\frac{\sqrt{\det\mathbf{G}_2^s(0)}}{\sqrt{\det\mathbf{G}_2^s(z_2)}}\exp\left(\frac{ik_1^p\Phi^p(z_2)}{2}\right) \quad \cdots\cdots (7)$$

The definitions of various terms in Eqs. (6) and (7) were discussed in detail by Schmerr (1998, 2000a; 2000b).

2.5. Corner Reflection of a Specimen

When the incident beam reflects right at the large corner of a specimen, the total length of the beam travel (as shown in Fig. 3 (a)) becomes the same as that of the case in Fig. 3 (b), where the beam reflects from the "normal" plane (to the refracted beam) located right at the corner. With taking advantages of this identity, one can calculate the corner reflection, $V_{cr}(\omega,\mathbf{x})$, with the model given in Eqs. (8) and (9), where the same reflection coefficient is multiplied twice.

$$V_{cr}(\omega)=\frac{\beta(\omega)}{S}\int_S v_{cr}(\omega,\mathbf{x})dS \quad \cdots\cdots (8)$$

where $v_{cr}(\omega,\mathbf{x})$ is given by:

$$v_{cr}(\omega,\mathbf{x})=\sum_{n=1}^{15}\frac{A_n}{1+\left(\frac{iB_n z_1}{x_r}\right)}T_{12}^{s;p}\left(R_{23}^{s;s}\right)^2 T_{21}^{p;s}\frac{\sqrt{\det\mathbf{G}_2^s(0)}}{\sqrt{\det\mathbf{G}_2^s(z_2)}}\frac{\sqrt{\det\tilde{\mathbf{G}}_3^s(0)}}{\sqrt{\det\tilde{\mathbf{G}}_3^s(z_3)}} \times\frac{\sqrt{\det\mathbf{G}_4^s(0)}}{\sqrt{\det\mathbf{G}_4^s(z_4)}}\exp(2ik_1 z_1)\exp\left(2ik_2^s z_2\right)\exp\left(\frac{ik_2^s\Phi^p(z_4)}{2}\right) \quad \cdots\cdots (9)$$

where $R_{23}^{s;s}$ is the reflection coefficient at the normal plane to the incidence wave.

2.6. Corner Reflection of a Surface Breaking Vertical Crack

The major contribution of corner trap signal of a surface breaking vertical crack (as shown in

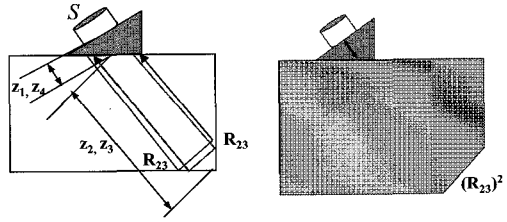

Fig. 3 (a) Geometrical setup for corner reflection, and (b) geometry of reflection from the normal plane to the incidence wave.

Fig. 4) comes from two ingredients. The first one is the reflection at the side of a vertical crack followed by the reflection at the bottom. The second one is the reflection at the bottom surface of the specimen followed by the reflection at the side of the vertical crack. Thus, the corner trap signal of a surface breaking vertical crack can be calculated by Eq. (10).

$$V_{vc}(\omega)=V_{side}(\omega)+V_{btm}(\omega) \quad \cdots\cdots (10)$$

where $V_{vc}(\omega)$ is the reflected velocity from the crack corner in the frequency domain, $V_{side}(\omega)$ is the reflected velocity through the vertical crack side firstly and from the specimen bottom lastly, and $V_{btm}(\omega)$ is the reflected velocity through the specimen bottom firstly and from vertical crack side lastly. $V_{side}(\omega)$ and $V_{btm}(\omega)$ are given by Eqs. (11) and (12), respectively.

$$V_{side}(\omega)=\beta(\omega)\int_{S_w}\int_0^{+f_D}\sum_{n=1}^{15}\frac{A_n}{1+\frac{iB_n z_1}{z_r}}\exp(ikz_1)\exp\left(ik_2^S z_2\right)\exp\left(ik_2^S z_3\right) \times\exp\left(ik_2^S z_4\right)T_{12}^{S;P}\left(R_{23}^{S;S}\right)^2 T_{21}^{P;S}\frac{\sqrt{\det\mathbf{G}_2^S(0)}}{\sqrt{\det\mathbf{G}_2^S(z_2)}} \times\frac{\sqrt{\det\tilde{\mathbf{G}}_3^S(0)}}{\sqrt{\det\tilde{\mathbf{G}}_3^S(z_3)}}\frac{\sqrt{\det\tilde{\mathbf{G}}_4^S(0)}}{\sqrt{\det\tilde{\mathbf{G}}_4^S(z_4)}}\frac{\sqrt{\det\mathbf{G}_5^S(0)}}{\sqrt{\det\mathbf{G}_5^S(z_5)}}\times\exp\left(\frac{ik_2^S\Phi^S(z_5)}{2}\right)dE_a dS_w \quad \cdots\cdots (11)$$

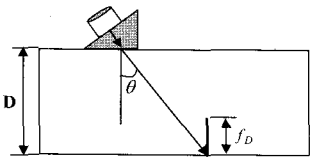

Fig. 4 A schematic representation of the angle beam UT of a vertical crack corner.

$$V_{him}(\omega)=\beta(\omega)\int_{S_w}\int_0^{-f_0/\tan\theta}\sum_{n=1}^{15}\frac{A_n}{1+\frac{iB_n z_1}{z_r}}\exp(ikz_1)\exp(ik_2^S z_2)\exp(ik_3^S z_3)$$
$$\times\exp(ik_2^S z_4)T_{12}^{S;P}\left(R_{23}^{S;S}\right)^2 T_{21}^{P;S}\frac{\sqrt{\det\mathbf{G}_2^S(0)}}{\sqrt{\det\mathbf{G}_2^S(z_2)}}$$
$$\times\frac{\sqrt{\det\tilde{\mathbf{G}}_3^S(0)}}{\sqrt{\det\tilde{\mathbf{G}}_3^S(z_3)}}\frac{\sqrt{\det\tilde{\mathbf{G}}_4^S(0)}}{\sqrt{\det\tilde{\mathbf{G}}_4^S(z_4)}}\frac{\sqrt{\det\mathbf{G}_5^S(0)}}{\sqrt{\det\mathbf{G}_5^S(z_5)}}\exp\left(\frac{ik_2^S\mathbf{\Phi}^S(z_5)}{2}\right)dE_a dS_w \quad \cdots\cdots(12)$$

where f_0 is the size of the crack, θ is the refracted angle of the beam, z_1 is the distance from transducer to the interface, z_2 is the distance from the interface to the vertical crack surface, z_3 is the distance from the vertical crack surface to the specimen bottom, z_4 is the distance from the specimen bottom to the interface and z_5 is the distance from interface to the transducer. The definitions of various terms can be found in Kim and Song (2002).

2.7. Isolated Flaw Signal

The ultrasonic testing signals that can be obtained by an angle beam transducer from isolated flaws such as a circular planar crack, a spherical void and a side-drilled hole can also be calculated by using Eq. (5). In the calculation of isolated flaw signals, however, one should adopt the proper far-field scattering amplitudes. For example, the far-field scattering amplitude from a circular crack, $A_{cr}(\omega)$, obtained by adopting the Kirchhoff approximation is given by Eq. (13) (Schmerr, 1998).

$$A_{cr}(\omega)=-\frac{ib^2 e_{sl}^p e_{sn}^p e_{sj}^p C_{kplj} D_p^p n_k}{2\rho_2\left(c_2^p\right)^2\left|\mathbf{e}_i^p-\mathbf{e}_s^p\right|r_e^{p;p}}J_1\left[k_2^p\left|\mathbf{e}_i^p-\mathbf{e}_s^p\right|r_e^{p;p}\right] \quad \cdots\cdots(13)$$

where b is the radius of the penny-shaped crack. The detailed definition of individual terms can not be addressedhere due to space limitation, but can be found in Schmerr (1998).

Based on the Kirchhoff approximation, the far-field scattering amplitude from a spherical void, $A_{SV}(\omega)$, can be obtained by Eq. (14).

$$A_{SV}(\omega)=\frac{-b}{2}\exp(-ik_{\alpha 2}b)\left[\exp(-ik_{\alpha 2}b)-\frac{\sin(k_{\alpha 2}b)}{k_{\alpha 2}b}\right] \quad \cdots\cdots(14)$$

where b is the radius of the spherical void.

The corresponding far-filed scattering amplitude for a 3-dimensional side-drilled hole of the length of ΔL, $A_{SDH}(\omega)$, can be given by Eq. (15) using the Kirchhoff approximation with the assumption of small size in its diameter (Schmerr and Sedov, 2002).

$$A_{SDH}(\omega)=\Delta L\frac{-ik_{\alpha 2}b}{2}\left\{H_1(2k_{\alpha 2}b)+iJ_1(2k_{\alpha 2}b)-\frac{2}{\pi}\right\} \quad \cdots\cdots(15)$$

where b is the radius of the side-drilled hole, and H_1 and J_1 are the Struve and Bessel functions of the first order, respectively.

2.8. Experimental Validation of the Models

It is worthwhile to note that the system efficiency factor should be defined for the experimental validation in time domain. For this purpose, the reflection signal from the circular part of the STB-A1 block was captured by use of a planar transducer with the center frequency of 5 MHz and the diameter of 0.375 inch as shown in Fig. 5 (a). Then, the system efficiency factor for a given ultrasonic testing system was determined as shown in Fig. 5(b).

Once the system efficiency factor is defined, the time domain waveforms expected to acquire can be predicted by the inverse Fourier transform of the ultrasonic testing models presented above. Fig. 6 shows the experimentally measured signal (with the same set-up as that for Fig. 5) from the

small counter bore (with the width of 4 mm) in the specimen together with the predicted time domain signal (using Eq. (5)). The excellent agreement between the theory and the experiments demonstrates the validity of the proposed model.

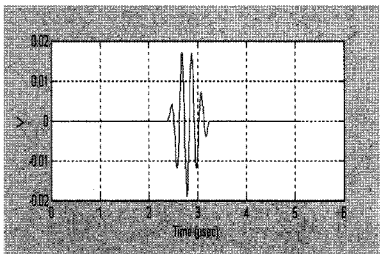

(a)

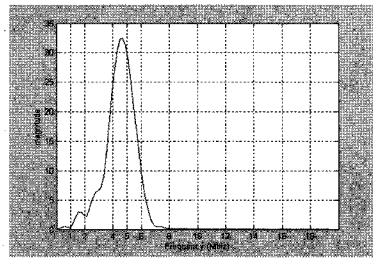

(b)

Fig. 5 (a) The experimental reference reflection signal, and (b) the system efficiency factor for a 5 MHz center frequency, 0.375 inch diameter transducer with the refracting angle of 45 degrees in the STB-A1 block.

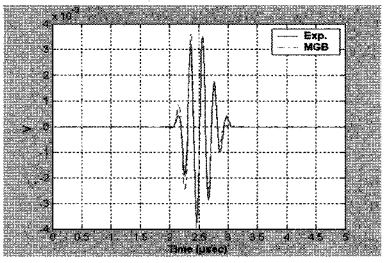

Fig. 6 Comparison of the experimentally measured signal to the predicted time domain signal from the small counter bore in the specimen. (Solid line: the experimental signal, Dotted line: calculated signal using multi-Gaussian beam model).

Figs. 7 (a) and (b) show similar comparisons between experimentally measured signals and predicted (using Eq. (8)) time domain waveformsof corner reflection from the specimens with the thickness of 25 mm and 29 mm, respectively. As shown in Fig. 7, the prediction agrees very well with the experiments.

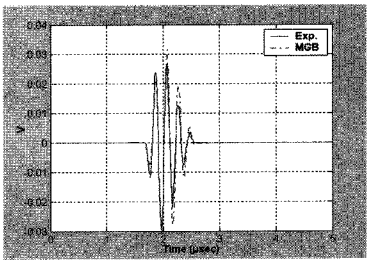

(a)

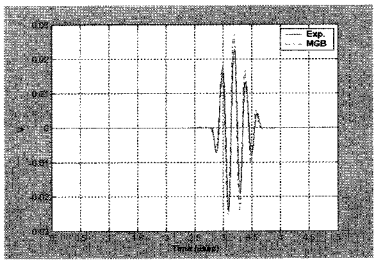

(b)

Fig. 7 Comparison of the predicted corner reflection signals to the experimental signals from the specimens with the thickness of (a) 25mm, and (b) 29 mm. (Solid line: experimental signal, Dotted line: calculation by use of the multi-Gaussian beam model)

The further comparisons between the model prediction and theexperimental measurement for other reflectors and scatterers are not shown here due to space limitation, since they can be found elsewhere (Kim and Song, 2002; Kim et al., 2002). In fact, they showed very good agreements demonstrating the high accuracy of the proposed models.

3. Model-based Identification of Crack Tip Signals

For the proper sizing of surface breaking vertical crack, the first task that needs to be taken care of is the identification of the crack tip signals from complicated UT signals. To solve this issue effectively, the TIFD (Technique for Identification of Flaw signals using Deconvolution) has been proposed previously (Song et al., 2002a; 2002b). The TIFD identifies flaw signals using a similarity function defined from the deconvolution of a target signal by a reference signal. The TIFD showed great potential to identify various practical signals, especially to distinguish notch signals from the geometric reflections. Unfortunately, however, the TIFD proposed in the previous work is not easy to implement for practical application, since it requires many reference signals. Obviously, it will be very difficult to acquire various reference signals in many situations.

Here, we introduce an enhancement of the TIFD based on the angle beam ultrasonic testing models in order to relax the requirement of acquiring various kinds of reference signals. Furthermore, the feasibility of the enhanced approach for the identification of crack tip signals is addressed. The enhanced approach adopts only one reference signal, which is the specular reflection from the circular part of the STB-A1 block. The deconvolution patterns of three different targets (including a corner, a counter bore, and a crack tip) are predicted using the proposed ultrasonic testing models.

Fig. 8 shows the calculated time-domain waveforms using the proposed angle beam UT models for three targets (such as a counter bore, a corner, and a crack tip) by use of the testing set-up whose efficiency factor is shown in Fig. 5. Here, it should be noticed that the crack tip signal (shown in Fig. 8(c)) is a flash point response from the leading edge of a circular crack as an approximate of the true crack tip diffraction signal, since the crack tip diffraction signal could not be calculated accurately by the Kirchhoff approximation.

Fig. 9 shows the calculated result of deconvolution patterns for three flaw signals (as shown Fig. 8) by adopting the specular reflection from the circular part of the STB-A1 block (as

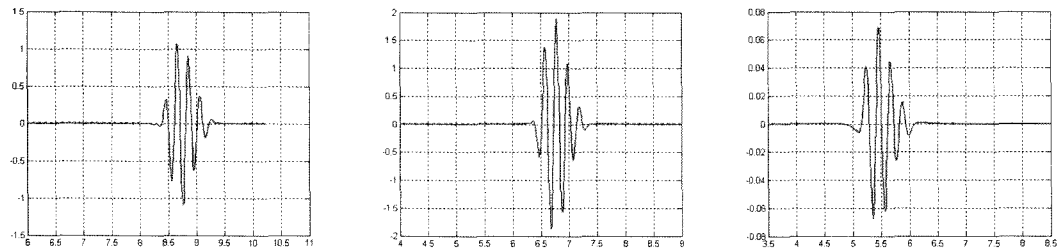

(a) (b) (c)

Fig. 8 Calculated time domain waveforms for (a) a counter bore, (b) a corner, and (c) a crack tip.

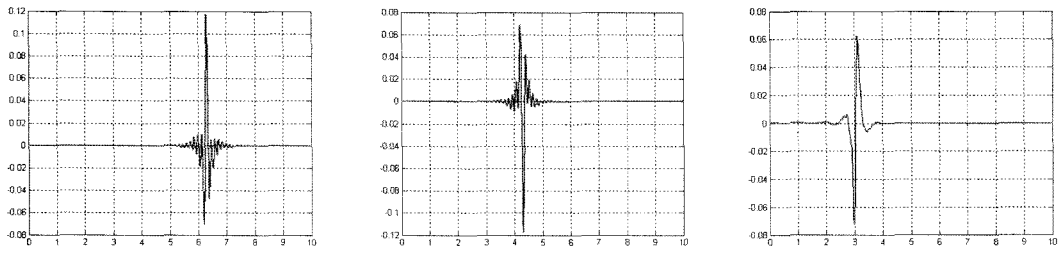

(a) (b) (c)

Fig. 9 Deconvolution patterns of calculated signals for (a) a counter bore, (b) a corner, and (c) a crack tip.

shown in Fig. 5(b)) as the reference signal. The time domain waveforms as shown in Fig. 8 cannot be distinguished from each other. The deconvolution patterns shown in Fig. 9, however, can be clearly distinguished even with a naked eye. As shown in Fig. 9 (a) the deconvolution pattern of the counter bore reflection signal shows the positive "impulse-like pattern", while that of a corner reflection signal does the negative "impulse-like pattern" (Fig. 9(b)). On the other hand, the deconvolution patterns of the crack tip signal shows the "bipolar pattern," as shown in Fig. 9 (c).

Here it should be noticed that the positive peaks of the test signal (the flaw signal) and the reference signal (the specular reflection from the STB-A1 block) were aligned in the time domain prior to the deconvolution in frequency domain. If this alignment step is omitted, the deconvolution patterns would be same as those in Fig. 9.

As shown in Fig. 9, the deconvolution pattern of a crack tip signal is quite different from those of the geometric reflectors (such as the counter bore and the corner). Thus, it is possible to identify the crack tip signals from geometric reflection using the model-based TIFD approach. The performance of the model-based TIFD approach for the realistic experimental signals will be reported shortly elsewhere.

4. Model-based Sizing of Surface Breaking Vertical Cracks

The sizing of a surface breaking vertical crack is, in fact, equivalent to the measurement of the distance between the crack tip and the crack corner. Thus, for sizing of cracks, it is essential to capture the crack tip signals. Unfortunately, however, the crack tip signals are usually very tiny so that it is not easy to acquire. On the contrary, the corner trap signal (that is the reflection from the corner of a surface breaking crack) is easy to capture, since they are much higher in amplitude. Therefore, if it is possible to estimate the crack size directly from the corner trap signal it would be very beneficial. Furthermore, the estimated crack size can be used as the priori information for crack tip location so that the crack tip location would become much easier. In the present work, we propose a quantitative sizing method for surface breaking vertical cracks based on the angle beam UT models.

If we define the amplitude ratio (named as amplitude-area (Aa) factor and defined in time-domain) of the crack corner trap signal (that can be predicted by Eq. (10)) to that of the specimen corner signal (which can be calculated by Eq. (8)), it would be given by Eq. (16).

$$A_a = \frac{\mathrm{P\text{-}P}(V_{vc}(t))}{\mathrm{P\text{-}P}(V_{cor}(t))} \times 100\,(\%) \qquad \cdots\cdots (16)$$

where A_a is the Aa factor, $\mathrm{P\text{-}P}(V_{vc}(t))$ is the peak-to-peak amplitude of the vertical crack corner trap signal in the time-domain, $\mathrm{P\text{-}P}(V_{cor}(t))$ is the peak-to-peak amplitude from the specimen corner reflection signal in the time-domain.

Using the Aa factor we can plot a theoretically constructed curve, named as the size-amplitude curve (SAC), from which the vertical crack sizing can be performed quantitatively. Fig. 10 shows two examples of the SACs constructed for the specimens with the heights of 10 mm and 15 mm. As shownin Fig. 10, the SACs are very similar in spite of the difference in the specimen heights.

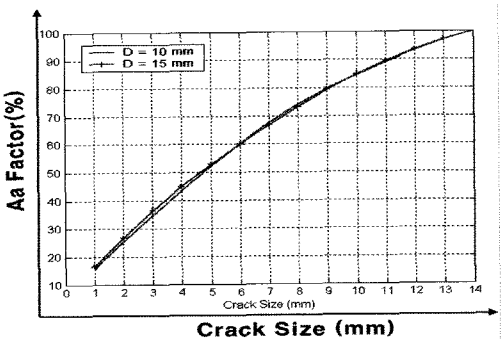

Fig. 10 Estimated the SACs for two specimens with different heights: transducer: 5 MHz center frequency, 0.375 inch diameter, and 45 degrees diffraction angle.

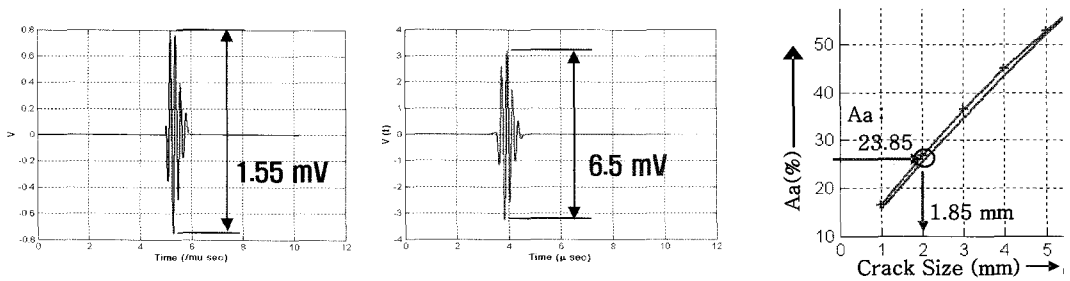

Fig. 11 (a) The experimentally measured corner trap signal from the 2 mm vertical crack, (b) predicted corner reflection signal from the 15 mm height specimen, and (c) the estimation of the vertical crack size using the SAC: Transducer 5 MHz center frequency, 0.375 inch diameter, and 45 degrees diffraction angle.

To demonstrate the sizing performance using the theoretically constructed SAC, we performed sizing of a surface breaking vertical crack (which is an artificial slit fabricated by electro-discharge machining) in a specimen with a height of 15 mm. Fig. 11 (a) shows the corner trap signal captured from the vertical crack corner, of which the peak-to-peak voltage is measured to be 1.55 mV. For the sizing of the surface-breaking crack using the SAC, we need to estimate the peak-to-peak voltage of the specimen corner. Fig. 11 (b) presents the result of the theoretical prediction (using Eq. (8)) of which the peak-to-peak voltage is calculated to be 6.5 mV. Then, we can calculate the Aa factor, which is turned out to be 23.85% in this particular example. Then, finally, we can estimate the unknown vertical crack size from the SAC, as shown in Fig. 11 (c), to be 1.95 mm. Considering the fact that actual size of the crack is 2.0 mm, one can recognize that the accuracy of the SAC sizing is very good.

However, it should be noticed some limitations of this approach. Firstly, this approach is valid only to open cracks. If cracks are closed it is necessary to adopt some other approaches, for example, addressed by Saka (2001). Secondly, this approach will not work for cracks of which the sizes are larger than the beam width of the transducer at the location of crack corner. In such a case, this approach will estimate the crack size merely as the beam width of the transducer.

5. Conclusions

Sizing of a surface breaking crack by angle beam ultrasonic testing involves two steps; the detection of the crack tip signal and the corner trap signal, and the measurement of the distance between them, which sounds very simple and straightforward. In many practical situations, however, it is not so easy since the angle beam ultrasonic testing signals are quite often captured together with non-relevant signals caused by geometric reflectors such as corners, counter bores and weld roots. To take care of this difficulty, we have proposed efficient and systematic approaches to the identification of the crack tip signals and the successive sizing of the surface breaking vertical cracks by use of the angle beam ultrasonic testing models that can predict the expected UT signals very accurately.

As the first application of the theoretical models, the model-based TIFD (Technique for Identification of Flaw signals using Deconvolution) has been proposed for the screening of the crack tip signals from the non-relevant geometric reflection signals, especially, counter bore signal and corner trap signal. As the second application, the

model-based Size-Amplitude Curve has been constructed for the reliable sizing of surface breaking vertical cracks. The performance of the proposed approaches was verified in the initial experiments, demonstrating the high possibility of their application in practice.

Acknowledement

This work was supported by grant No. 2000-2-30400-013-3 from the Korea Science & Engineering Foundation.

Rererences

Kim, H. J. and Song, S. J. (2002) Prediction of Angle Beam Ultrasonic Testing Signals Using Multi-Gaussian Beams, in: D. O. Thompson and D. E. Chimenti (Eds.), Review of Progress in quantitative Nondestructive Evaluation, Vol. 21A, American Institute of Physics, Melville, New York, pp. 839-846

Kim, H. J., Song, S. J. and Kim, Y. H. (2002) Quantitative Approaches to Flaw Sizing Based-on Ultrasonic Testing Models, Review of Progress in Quantitative Nondestructive Evaluation, Bellingham, Washington, July 14-19

Saka, M. (2001) Sensitive NDE of Small Fatigue Cracks, Journal of the Korean Society for Nondestructive Testing, Vol. 21, No. 1, pp. 22-31

Schmerr, L. W. (1998) Fundamentals of Ultrasonic Nondestructive Evaluation - A Modeling Approach, Plenum, New York

Schmerr, L. W. (2000a) A Multigaussian Ultrasonic Beam Model for High Performance Simulations on a Personal Computer, Materials Evaluation, Vol. 58, No. 7, pp. 882-888

Schmerr, L. W. (2000b) Lecture Note on Ultrasonic NDE Systems Models and Measurements, Sungkyunkwan University, Suwon, Korea

Song, S. J. and Kim, H. J. (2000) Modeling of Radiation Beams from Ultrasonic Transducers in a Single Medium, Journal of the

Korean Society for Nondestructive Testing, Vol. 20, No. 2, pp. 91-101 (in Korean)

Song, S. J., Kim, J. Y. and Kim, Y. H. (2002a) Identification of Flaw Signals in the Angle Beam Ultrasonic Testing of Welded Joints with Geometric Reflectors, in: D. O. Thompson and D. E. Chimenti (Eds.), Review of Progress in quantitative Nondestructive Evaluation, Vol. 21A, American Institute of Physics, Melville, New York, pp. 691-698

Song, S. J., Kim, J. Y. and Kim, Y. H. (2002b) Identification of Flaw Signals Using Deconvolution in Angle Beam Ultrasonic Testing of Welded joints, Journal of the Korean Society for Nondestructive Testing, Vol. 22, No. 4, pp. 422-429 (in Korean)

Thompson, R. B. and Gray, T. (1983) A Model Relating Ultrasonic Scattering Measurements through Liquid-Solid Interfaces to Unbounded Medium Scattering Amplitudes, Journal of Acoustical Society of America, Vol. 74, pp. 1279-1290